Springer

Journal of Mechanical Science and Technology 22 (2008) 1800~1807

Journal of Mechanical Science and Technology

www.springerlink.com/content/1738-494x
DOI 10.1007/s12206-008-0612-5

Comparison between numerical computations and measurements by LDV for fluid flow in rectangular duct systems

Kyung Hwan Kim[1,*], Jin Gi Paeng[2] and Young Hwan Yoon[2]

[1]*Division of Facilities, Changwon National University*
[2]*Department of Mechanical Engineering, Changwon National University*

(Manuscript Received January 10, 2008; Revised June 5, 2008; Accepted June 17, 2008)

Abstract

Fluid flows in rectangular duct systems are measured by using the laser-Doppler velocity meter and computed by commercial software of Star-CD for comparisons between flows. Three rectangular systems are investigated in this study: a rectangular duct with a 90 degree bent elbow, a rectangular duct with two branches, and a rectangular duct in the middle of which a circular cylinder is located. These investigations show that the numerical solutions satisfactorily predict design factors: for example, the K -factor for an elbowed duct, the distribution ratio of flow rates into each branch from a main duct, and the Nusselt number around the circular duct. However, there are some disagreements in the velocity profile and turbulent kinetic energy at each cross section of the duct systems.

Keywords: 90 degree banded elbow; Branch duct; Circular cylinder; Heat transfer; Turbulent kinetic energy; Numerical computation; Experimental measurement

1. Introduction

Recent increases in demands for energy generation, utilization, and conservation have resulted in the need to design a higher capacity and more efficient energy system. In order to obtain optimum design and operating conditions, several commercial softwares for the numerical computations have been employed in many engineering problems.

However, the numerical simulations are satisfactory for simple geometries in which analytic solutions may exist or some specific engineering problems. But, in the literature, there have not been many cases that researchers check the exactness by comparing their numerical solutions to experimental data. For example, Hinchcliffe and Haidar [1] computed distribution of flow rates in an automobile air conditioner duct system without comparison of their numerical results with experimental data. Shiroyama et al. [2] also designed a automobile air conditioner duct with no comparisons with measurements. In the other way, Kim [3] and Kim and Kim [4] computed three-dimensional fluid flows in a duct and a wind tunnel, respectively, in order to compare their solutions with experimental data from other papers.

Furthermore, exactness or good simulation of the numerical programs depends on inlet boundary condition. Even in computation of complex systems in the literature, inlet boundary conditions are unknown. For an instance, Kang and Hong [5] assumed mean velocity profiles as inlet condition in their paper.

Besides the mean velocity at the inlet, turbulent intensity may affect numerical solutions. Zhukauskas and Ziugzda [6] reported that turbulent intensity increased the heat transfer coefficient in the heat transfer system. But, Cho et al. [7] assumed simply that the mean turbulent fluctuation velocity is 30% of mean velocity at inlet. Lee et al. [8] gave assumed constants to inlet conditions of turbulent kinetic energy, K and turbulent dissipation energy, ε in the paper.

However, in this paper, the fluid flows, including mean velocities and turbulent fluctuations in rectangular

*Corresponding author. Tel.: +82 55 213 2147, Fax.: +82 55 213 2159
E-mail address: c9837@changwon.ac.kr

duct systems are measured by using the laser-Doppler velocity meter and computed with commercial software, under local boundary conditions known from measurements, so that comparisons between them can be made.

This paper introduces three cases: a rectangular duct with a bent elbow by Yoon and Park [9], a rectangular duct with two branches by Yoon et al. [10], and a cylinder in a rectangular duct by Kim and Yoon [11]. Through these problems, the mean velocity, the turbulent components, and several design outputs are discussed with comparisons via numerical computations and measurements.

From this study, it can be said that numerical solutions simulate some design parameters satisfactorily. Those are the K-factor for frictional coefficient in ducts, distribution of flow rate in duct system, and heat transfer coefficient obtained by integration through a certain area.

2. Experiments and methods

Experiments with three duct systems are introduced in this paper. The first system is a rectangular duct with bent elbow, as shown in Fig. 1. In this figure, a fan blows air into a duct and it passes through a gradual contraction to a right-angle rectangle. The air flow rate is controlled with an inverter by changing the fan speed. After the contraction, water particles from an electric humidifier are introduced into the duct at the top and bottom plates. The mixture of air and water particles then passes through a duct with a bent elbow. Measuring section of the duct from a bended elbow is made of glass as shown in the figure so that a laser beam can penetrate into the flow fields inside the duct. The laser beam senses the velocities of the water particles in air. Flow fields are measured at cross sections before and after the bent elbow by a laser transmitter. The second system is identical to the first except that two branch ducts exist at exit instead of a bent duct, as shown in Fig. 2. The last system is such that an electrically heated brass rod is located in the middle of a straight duct. Measurements of air velocities are made at the upstream inlet cross section, the middle cross section of the rod, and the downstream exit cross section of the duct.

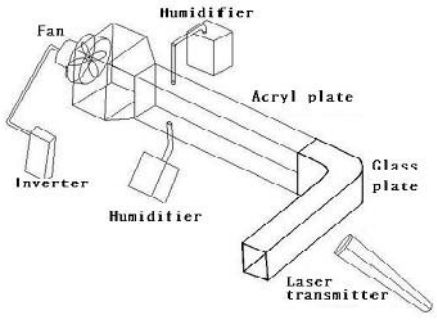

Fig. 1. Schematic diagram of the experimental apparatus for an elbowed rectangular duct.

3. Numerical analysis

3.1 Governing equation

A continuity equation and a momentum equation for the flow field are given in Eq. (1) and Eq. (2), respectively.

$$\frac{\partial U_i}{\partial X_i} = 0 \tag{1}$$

$$U_j \frac{\partial U_i}{\partial x_j} = -\frac{1}{\rho}\frac{\partial p}{\partial x_i} + \frac{\partial}{\partial x_j}\left(\nu \frac{\partial U}{\partial x_j} - \overline{u_i' u_j'}\right) \tag{2}$$

The turbulent stress term $-\overline{u_i' u_j'}$ of Eq. (2) is defined as Eq. (3)

$$-\overline{u_i' u_j'} = \frac{2}{3}\delta_{ij}k + \frac{\mu_t}{\rho}\left(\frac{\partial u_i}{\partial x_j} + \frac{\partial u_j}{\partial x_j}\right) \tag{3}$$

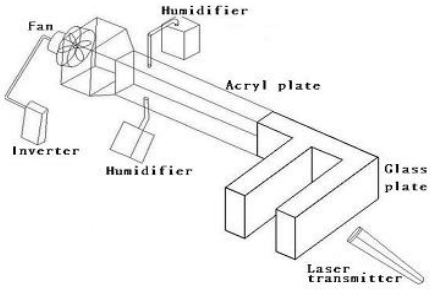

Fig. 2. Schematic diagram of the experimental apparatus for a rectangular duct with two branches.

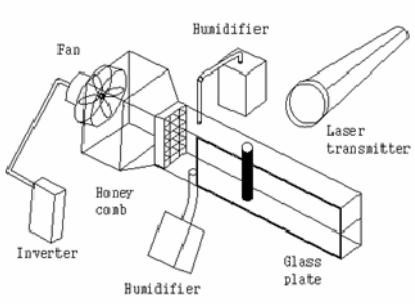

Fig. 3. Schematic diagram of the experimental apparatus for a cylinder in a rectangular duct.

where μ_t is the turbulent viscosity defined as Eq. (4) with the turbulent kinetic energy, K, and the turbulent dissipation energy, ε.

$$\mu_t = C_\mu \rho \frac{K^2}{\varepsilon} \tag{4}$$

3.2 Boundary condition

As the fluid flow in the control volumes is three-dimensional, steady state, and because it is a turbulent flow, the computation needs to solve three velocity components (U, V, W), as well as K and ε for the turbulence.

The principal velocity U_{in} and its perpendicular velocity component W_{in} are measured with the laser velocity meter for the inlet boundary condition. However, V_{in} is assumed to be zero as it is the smallest component at the inlet from the geometry of the inlet rectangle.

The turbulent kinetic energy K at the inlet is written as

$$K = \frac{1}{2}(\overline{u'^2} + \overline{v'^2} + \overline{w'^2}) \tag{5}$$

Turbulent components, $\overline{u'^2}$ and $\overline{w'^2}$ of Eq. (5) are measured with the laser-Doppler velocity meter at the inlet, but $\overline{v'^2}$ at the location is assumed to be nearly equal to $\overline{w'^2}$ such that

$$K = \frac{1}{2}(\overline{u'^2} + 2 \cdot \overline{w'^2}) \tag{6}$$

Turbulent dissipation energy ε at the inlet is also obtained from the following relationship:

$$\varepsilon = C_u^{0.75} \times \frac{K^{1.5}}{l} \tag{7}$$

Here, the turbulent mixing length l assumed to be 10% of the smaller width of the inlet rectangular cross section.

A non-slip condition is applied for all walls, such as

$$U_{wall} = V_{wall} = W_{wall} \tag{8}$$

Finally, the zero pressure condition is given at the exit as

$$P = 0 \tag{9}$$

4. Results and considerations

4.1 Rectangular duct with bent elbow

Velocity vectors from the computations are presented in (a) of Fig. 4; in addition, (b) in the figure represents coordinate systems (x, y, z) at the inlet, the middle section 19 cm from the inlet wall, and the exit section 19x2 cm from the inlet wall. The dimension of the cross section is 6 cm x 20 cm.

In Fig. 5, experimental data and numerical results for the principal velocity, U at the inlet, middle, and exit section described at (b) of Fig. 4 are shown. The first graph of (a) for the inlet represents velocity profiles at z = 5 cm (see (b) of Fig. 4). The second and third graphs of (a) are the velocity profiles at z = 10 and 15 cm, respectively. Graphs for (b) middle section and (c) exit also show the velocity profiles in the same way for Re = 11,643, 19,716, and 24,260, as shown in the legend. All velocity profiles at the inlet are measured with the velocity meter, while the velocity profiles from both experiments and the computations are drawn in the figures in the middle and at the exit sections. It is shown that the velocity becomes slower as y approaches zero, indicating the inner wall of curvature at the middle section. The inside velocity then becomes faster and the outside velocity slower. Eventually, velocity profiles tend to become normal distribution at the exit. It can be said that the computation makes a relatively good simulation of the experiments. Relative errors between the experiment and the computation range from 0.51% to 19.17% with a mean relative error of 7.71%.

(a)

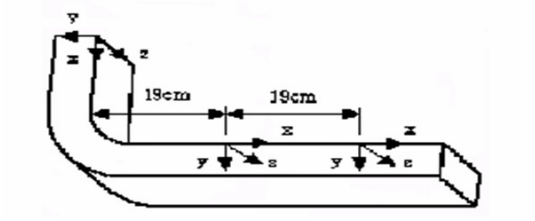

(b)

Fig. 4. Computation result of the velocity vectors and axis representation for distributions of the fluid flow at each cross-section.

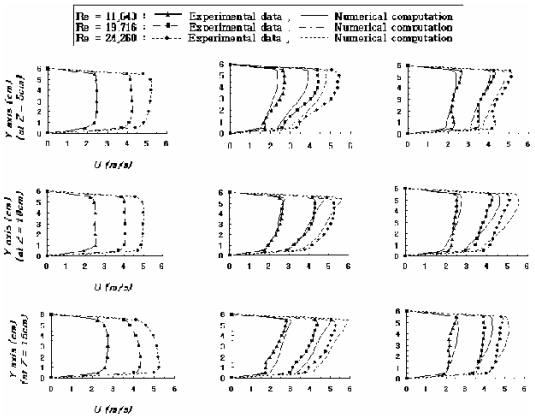

(a) Inlet (b) Middle section past elbow (c) Exit

Fig. 5. Comparison of the x-direction velocity (U) between the experimental data and the 3-D computation data.

Fig. 6 presents the turbulent kinetic energy by numerical computation in addition to that by an experimental measurement. The arrangement and the notations in the graphs are identical to those in Fig. 5. Profiles of the turbulent kinetic energy at the inlet are measured as (a) of Fig. 6. At the middle section past the elbow and the exit section, the experimental data (marked lines) and the numerical computation (dotted lines) are compared to each other at various Reynolds numbers. At the middle section past the elbow, the experimental turbulent kinetic energy becomes greater at the inner curvature, indicating that z is approaching zero. In contrast, the computed turbulent kinetic energy becomes greater at the outer curvature indicating that z is approaching 6 in Fig. 6. It appears that the experimental turbulent kinetic energy becomes greater, as the eddy current is transported from the upstream elbow. However, the numerical results directly contrast with the experiments at this middle section. At the exit section, the magnitudes of the turbulent kinetic energy from both the numerical computation and experimental results become smaller due to the characteristics of turbulence as the fluid flows downstream. In addition, it was observed that the magnitude of the turbulent kinetic energy is proportional to the Reynolds number for all cases in Fig. 6. For reference, the relative errors of the numerical computations to the experiments for the turbulent kinetic energy range from 0.12 to 81.78% with an average error of 33.74%.

The K-factor of the duct elbow is computed from the data of the numerical computation with Eq. 10 as Fig. 7. In the figure, the K-factor is compared with the experimental data of Wirt [12] and the design data of ASHRAE [13] for the same ratios of the duct sides and

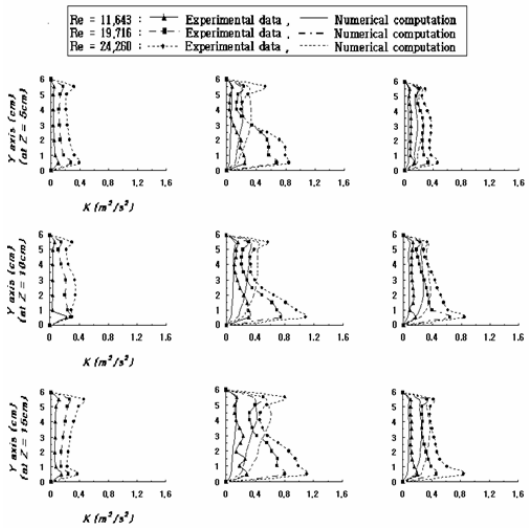

(a) Inlet (b) Middle section past elbow (c) Exit

Fig. 6. Distribution of turbulent kinetic energy K.

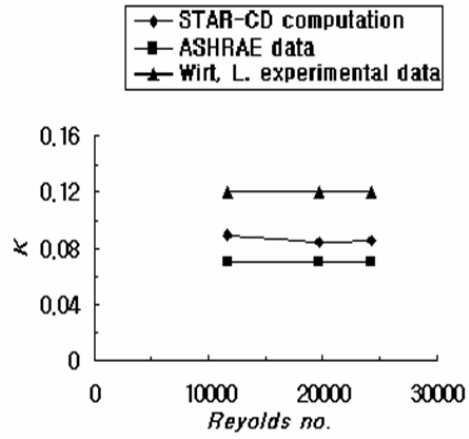

Fig. 7. Friction factor.

the curvature of the elbow. It was found that the K-factor from the numerical computation is located between the lines of the data from Wirt and ASHRAE.

$$K = \frac{\Delta P \cdot 2}{V_m^{\,2} \cdot \rho} \tag{10}$$

4.2 Rectangular duct with two branches

An example of the computed velocity vectors was drawn in the computational domain of a rectangular duct with two branches, as shown in Fig. 8.

The percentages of the flow rate to each branch are presented with various Reynolds number in Fig. 9. In

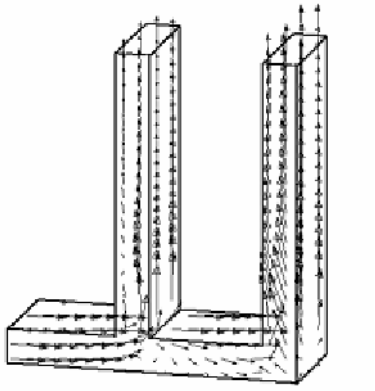

Fig. 8. Computational result in a duct with two branches.

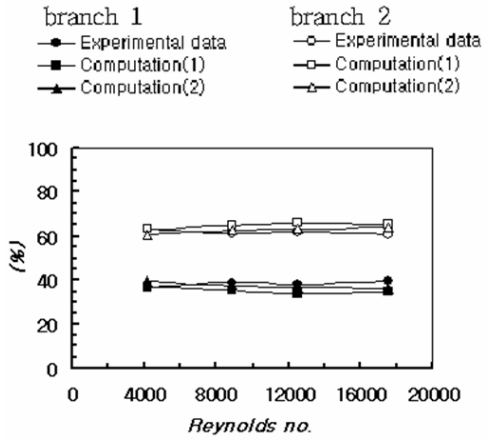

Fig. 9. Percentage of the flow rates at each branch of the duct system.

this figure, branch 1 and branch 2 represent the upstream branch and the downstream branch from main duct, respectively. Furthermore, computation (1) is a case in which the experimental velocity profile is used as the inlet boundary condition for the computation. On the other hand, computation (2) is a case in which the uniform velocity profile with the same flow rate as the computation (1) is used as the inlet boundary condition. If the flow rate of the main duct is 100%, an average of 37.65% of total flow flows into branch 1 and an average of 62.23% of the total flow rate flows into branch 2 in the figure. It is also shown that the distribution ratio into each branch is nearly invariant to the Reynolds number for both experiments and the computations. The errors of the distribution ratio range from 0.3 to 4.77% for computation (1), from 1.2 to 3.14% for computation (2). Therefore, it can be said that both computations simulate the distribution ratios of the experiments well.

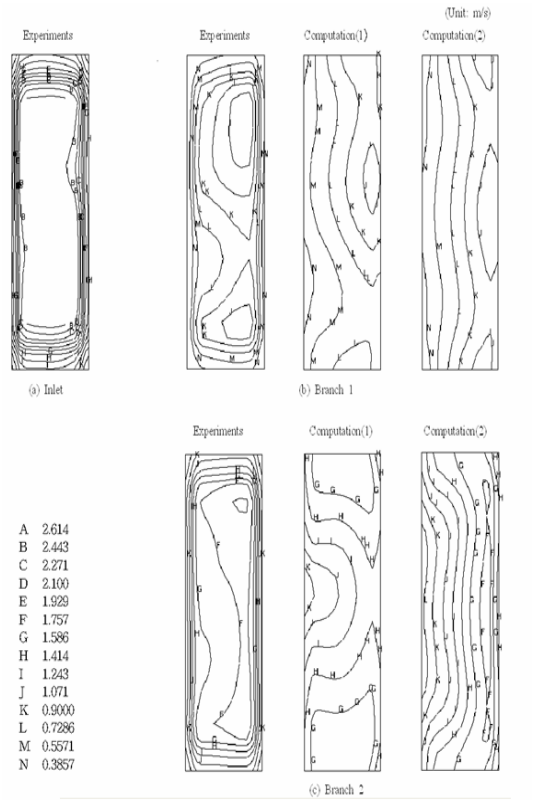

Fig. 10. Contours of experimental and computed velocity profiles at each branch (Re=12.532) Computation (1): computation with measured inlet velocity profile, Computation (2): computation with uniform inlet velocity profile.

Fig. 10 shows the velocity contours at each cross section of the duct system for a Reynolds number of 12,532. This figure consists of three parts. The first part of (a), the inlet, shows the velocity contours from the experiments at the inlet of the computational domain. The second part is (b), branch 1, in which three velocity contours are given from the experiments, computation (1), and computation (2) at the exit cross section of branch 1. The last part (c) of the figure represents the velocity contours at the exit cross section of branch 2 in the same way with part (b). Differences can be observed in the shape of the contour between the experiments and computations. There are also differences between the contours of computation (1) and computation (2).

4.3 Fluid flow past a cylinder in a rectangular duct

The fluid flow and heat transfer were measured and computed around a cylinder in a rectangular duct, as shown earlier. Fig. 11 shows the principal velocity

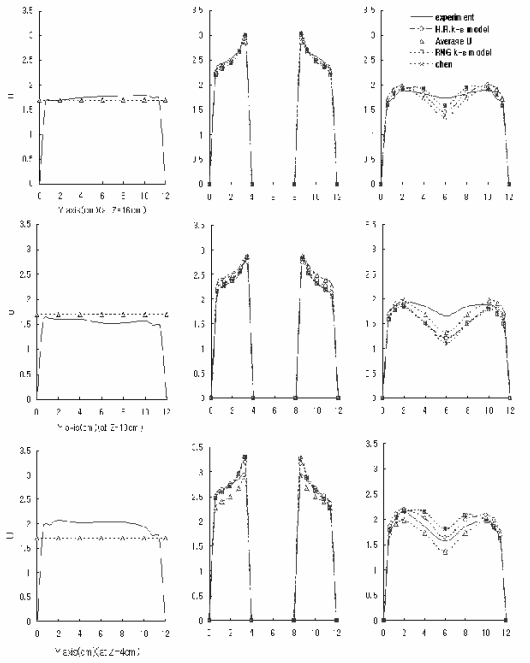

Fig. 11. Comparison of x-direction velocity, U[m/s] between the experimental data and the3 -D computation data.

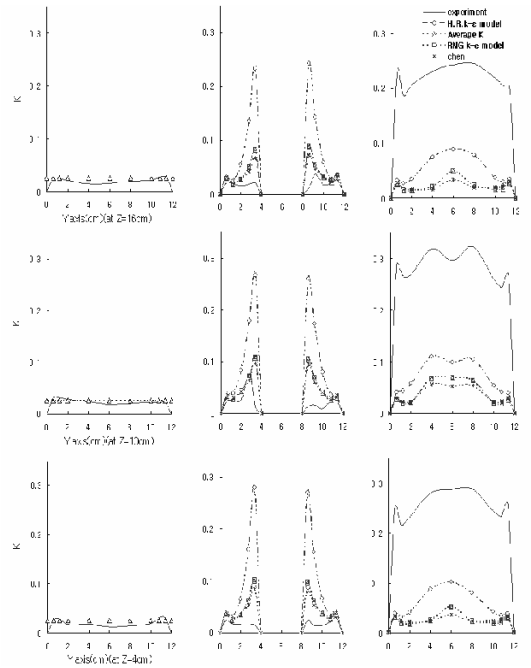

Fig. 12. Distribution of the turbulent kinetic energy.

component, U at each cross section of the duct with a Reynolds number of 4,457 based on the diameter of the circular cylinder and the mean velocity at the inlet cross section. Graphs of the first column in the figure present principal velocity profiles at z = 4, 10, and 16 cm of inlet cross section. For reference, the height and width of the duct is z = 20 cm and x = 10 cm, respectively, where the solid lines are the measured velocity profiles and the straight lines with triangular marks (Δ) are the mean velocity profiles obtained from the measurement. Graphs of the second column, the middle section, present principal velocity profiles at both passages between the cylinder and each wall of the duct in which a circular cylinder is located at x = 4 to 6 cm. These graphs show the measured velocity profiles (solid lines) and computed velocity profiles with the standard $K-\varepsilon$ model, the RNG $K-\varepsilon$ model, and Chen's $K-\varepsilon$ model. All velocity profiles from the measurements and the computations are shown as close to each other, and the velocity becomes faster close to the wall of the cylinder at x = 4 and 6 cm. The last graphs of the last column, the exit section, present the velocity profiles in the wake region behind the cylinder. It appears that the computed profiles simulate the measured lines (solid line) while some differences exist between them behind the center of the cylinder at x = 6 cm.

Fig. 12 shows measured and computed turbulent kinetic energy, K, at the same condition and representation with Fig. 11. When evaluating the measured turbulent kinetic energy, it is assumed $\sqrt{w'^2}$ is equal to $\sqrt{v'^2}$ because only $\sqrt{u'^2}$ and $\sqrt{v'^2}$ are measured by laser velocity meter. Graphs of the first column, inlet, present measured turbulent kinetic energy (solid line) which are almost uniform because of upstream honeycomb. Graphs of the second column, middle section, present turbulent kinetic energy at both sides of circle (x = 4 to 6 cm). It is seen that the computed value becomes higher to the wall of the cylinder (x = 4 & 6 cm). But the magnitude of the measured turbulent kinetic energy is much smaller than the computed values. Furthermore, there is no significant tendency to make turbulence higher to the wall of the cylinder. Graphs of the last column, exit section, present turbulent kinetic energy in the wake region behind the cylinder. It can be seen that turbulence occurs highly past the cylinder from solid lines (measured one). However, computed values predict turbulence much smaller than that of the measured value.

Fig. 13 shows the average Nusselt numbers of the cylinder when the cylinder is heated with an inside electric wire. The experiment (with white circle) in the legend is the measured Nusselt number from the electric power supplied to the cylinder. All other lines in the figure are computed Nusselt numbers for comparison with the

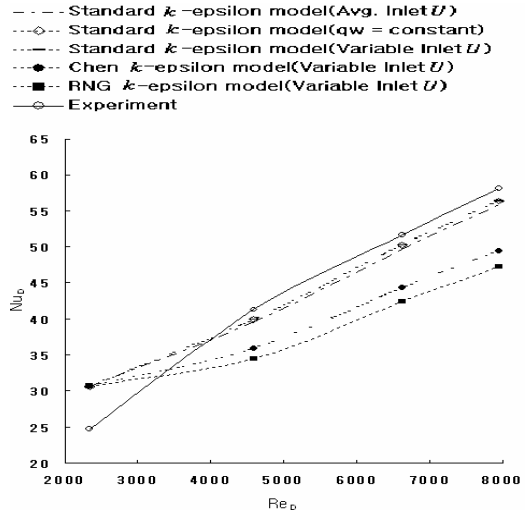

Fig. 13. Comparison of average Nusselt number between experiment and numerical computation.

measured Nusselt number. First, variable Inlet U indicates computed Nusselt number with inlet boundary condition of variable velocity profile from the measurement. Second, Avg. Inlet U in the legend indicates the Nusselt number with average velocity profile at the inlet of the duct. Lastly, q_w = const is the case in which the constant heat flux boundary condition is used for the cylinder wall; on the other hand, the temperature boundary condition at the cylinder wall is used for the other computational cases.

If experimental Nusselt numbers are compared with the computed Nusselt numbers, there is a relatively large difference in the relative error, from 23.9% to 24.1%, when Re_D = 2,337. For the range of Reynolds numbers from 4,598 to 7,944, nearly the same range of relative errors exists for three cases of the standard $K-\varepsilon$ model (Avg. Inlet U), the standard $K-\varepsilon$ model (Variable Inlet U), and the standard $K-\varepsilon$ model (q_w = const): from 3.8 to 4.0%, 2.6 to 3.2%, and 2.6 to 4.0%, respectively. However, Chen's $K-\varepsilon$ model (Variable Inlet U) and the RNG $K-\varepsilon$ model (Variable Inlet U) have relatively large error ranges from 13.0 to 15%, and 16.4 to 18.7%, respectively. Therefore, the numerical computations with the Nusselt numbers simulate the experimental Nusselt numbers within 4.0%, except in the cases of the Chen and RNG models.

5. Conclusions

Fluid flows in three rectangular duct systems are reviewed by using comparisons between measurements with LDV and numerical computations with commercial software. The systems in this study are a rectangular duct with a 90 degree bent elbow, a rectangular duct with two branches, and a rectangular duct in the middle of which a circular cylinder is located. From these studies, the following conclusions are summarized.

(1) For the case of the rectangular duct with a 90 degree elbow, there is relatively good agreement in the principal velocity between the measurements and numerical computations. However, significant disagreements were noted in the turbulent kinetic energy levels between them. However, the K - factor from the numerical computation appears satisfactory in a comparison with the ASHRAE data as well as the experimental data from the literature.

(2) In the case of the rectangular duct with two branches, the computed velocity contour at the exit of each branch differs from the measured velocity contour at the same cross section. However, numerical simulations for the distribution ratio to each branch are feasible compared to the measurements of the ratio.

(3) For the fluid flow past the cylinder in a rectangular duct, disagreements in the velocity and turbulent kinetic energy levels in the wake region behind the cylinder were found between the numerical computations and the measurements. However, there was good agreement between them for the Nusselt numbers of the heated cylinder.

(4) From these considerations about the three systems, although there were disagreements in the velocity profile and turbulent kinetic energy values of the numerical computations compared to the measurements, these findings are relatively satisfactory in terms of the simulations of design factors of the K - factor through the elbow of the duct, the distribution ratio of the flow rate to each branch, and the Nusselt numbers of the heated cylinder. These are integrated values through a certain area.

Acknowledgments

This work is financially supported by the Ministry of Education and Human Resources Development(MOE), the Ministry of Commerce, Industry and Energy (MOCIE) and the Ministry of Labor(MOLAB) through the fostering project of the Industrial-Academic Cooperation Centered University

References

[1] S. Hinchcliffe and N. Haidar, CFD investigation into LD100 HVAC ducting system, Technical Review.

(1998) 145-152.

[2] M. Shiroyama, T. Ijawa and T. Hasegawa, Development of compact air conditioning for vehicle using CFD, J. of Mitsubishi Heavy Industry. 35 (2) (1998) 108-111.

[3] H. M. Kim and K. Y. Kim, A study on turbulence model for the analysis of 3-dimensional flow, Proceedings of The SAREK, Winter Annual Conference. (1998) 384-389.

[4] S. H. Kang and K. H. Hong, A numerical study on the laminar convective heat transfer around a circular cylinder in a uniform cross flow of liquid, Proceedings of the Korean journal of Air-Conditioning and Refrigeration Engineering. 8 (1) (1996) 26-36.

[5] J. T. Kim, Steady and unsteady flows with pressure-based unstructured Navier-Strokes solver PUNS, Korean Society of Computational Fluids Engineering, Spring Annual Conference. (1999) 98-105.

[6] A. Zhukauskas and J. Ziugzda, Heat transfer of a cylinder in cross-flow, Hemisphere Publishing Corporation, (1985).

[7] N. H. Cho and M. R. Kim, Numerical investigation of fluid flows in an automotive HVAC module, Technical Review. (1998) 125-135.

[8] J. H. Lee, B. J. Kim, D. J. Cho and S. J. Yoon, Effect of a variation of a main duct area on flow distribution of each branch, Korean Journal of Air-conditioning and Refrigeration Engineers. 17 (4) (2005) 386-395.

[9] Y. H. Yoon and W. G. Park, Study on velocity measurement and numerical computation in a rectangular duct with 90 bend elbow, Korean Journal of Air-Conditioning and Refrigeration Engineering. 15 (12) (2003) 910-917.

[10] Y. H. Yoon, T. H. Bae and W. G. Park, Experimental and computational studies for flow distribution in a rectangular duct system with two branches, Korean Journal of Air-Conditioning and Refrigeration Engineering. 14 (9) (2002) 766-733.

[11] K. H. Kim and Y. H. Yoon, Study on measurement and numerical analysis for fluid past a circular cylinder in rectangular duct, Korean Journal of Air-Conditioning and Refrigeration Engineering. 15 (12) (2003) 1095-1102.

[12] L. Wirt, General Electric Rev. 30 (6) (1927) 286.

[13] ASHRAE Hand BOOK, Fundamentals, (1977).